Competing Spin Liquid States in the Spin-$1/2$ Heisenberg Model On Triangular Lattice

Wen-Jun Hu, Shou-Shu Gong,* Wei Zhu, and D. N. Sheng
Department of Physics and Astronomy, California State University, Northridge, California 91330, USA

We study the spin-$1/2$ Heisenberg model on the triangular lattice with the antiferromagnetic first (J_1) and second (J_2) nearest-neighbor interactions using density matrix renormalization group. By studying the spin correlation function, we find a 120° magnetic order phase for $J_2 \lesssim 0.07J_1$ and a stripe antiferromagnetic phase for $J_2 \gtrsim 0.15J_1$. Between these two phases, we identify a spin liquid region characterized by the exponential decaying spin and dimer correlations, as well as the large spin singlet and triplet excitation gaps on finite-size systems. We find two near degenerating ground states with distinct properties in two sectors, which indicates more than one spin liquid candidates in this region. While the sector with spinon is found to respect the time reversal symmetry, the even sector without a spinon breaks such a symmetry for finite-size systems. Furthermore, we detect the signature of the fractionalization by following the evolution of different ground states with inserting spin flux into the cylinder system. Moreover, by tuning the anisotropic bond coupling, we explore the nature of the spin liquid phase and find the optimal parameter region for the gapped Z_2 spin liquid.

PACS numbers: 73.43.Nq, 75.10.Jm, 75.10.Kt

arXiv:1504.00654v2 [cond-mat.str-el] 3 Aug 2015

Quantum spin liquids (SLs) are long-range entangled states with remarkable properties of fundamental importance [1]. The SL physics has been considered to be essential to understand strongly correlated systems and unconventional superconductivity [2, 3]. The simplest and perhaps most striking SLs are the gapped topological SLs, which develop a topological order [4–6] with the emergent fractionalized quasiparticles [7–9]. Although SLs have been studied intensively for two decades and demonstrated in contrived models [10–20], the microscopic condition for the emergence of SLs in frustrated magnetic systems is not well understood.

At the experimental side, possible SLs have been discovered in various materials. Among these materials, the most promising systems are the kagome antiferromangets including the Herbertsmithite and Kapellasite [21–25], as well as the organic Mott insulators with a triangular lattice structure such as κ-$(ET)_2Cu_2(CN)_3$ [26–29] and $EtMe_3Sb[Pd(dmit)_2]_2$ [30, 31]. In all these materials, no magnetic order is observed at the temperature much lower than the interaction energy scale. These experimental findings have inspired intensive theoretical studies on the frustrated magnetic systems with strong frustration or competing interactions.

Theoretically, the kagome Heisenberg model appears to possess a robust SL. Density matrix renormalization group (DMRG) studies suggest a gapped SL [32–35], which may be consistent with a Z_2 topological order [34, 35]. Variational studies based on the projected fermionic parton wave functions however favor a gapless Dirac SL [36–38]. Interestingly, by introducing the second and third neighbor couplings [39–41] or the chiral interactions [42], DMRG [40–42] studies recently discovered another topological SL — chiral spin liquid (CSL) [43, 44], which breaks time reversal symmetry (TRS) spontaneously and is identified as the $\nu = 1/2$ bosonic fractional quantum Hall state. On the other hand, the non-magnetic phases in the frustrated honeycomb and square J_1-J_2 models appear to be conventional valence-bond solid state [45–48].

The spin-$1/2$ triangular nearest-neighbor antiferromagnetic (AF) Heisenberg model was the first candidate proposed to realize a SL ground state by Anderson [2], although it turns out to still exhibit a 120° AF order [49–53]. To understand the triangular weak Mott insulator materials, combined theoretical and numerical studies [54–56] on a spin model with four-site ring-exchange couplings [57] find a gapless *spin bose metal* with spinon Fermi sea. To enhance frustration [58–68], one way is to include the second-neighbor coupling J_2, where a stripe ordered state is found with larger J_2 coupling [58, 59], and an intermediate non-magnetic region may emerge [60–63] based on different approaches. The variational Monte Carlo simulations find a nodal d-wave SL [61] and a gapless SL [62] as the candidates for this intermediate phase, although such method has the enhanced tendency of finding fractionalized phase in nonmagnetic region. Very recently, a DMRG work [69] found the indication of a gapped SL which conserves the TRS in the non-magnetic phase. However, the nature of the quantum phase with the intermediate J_2 remains far from clear.

In this Letter, we study the spin-$1/2$ triangular model with the AF first and second nearest-neighbor $J_1(J_1')$-J_2 couplings based on DMRG calculations. The model Hamiltonian is given as

$$H = J_1 \sum_{\langle i,j\rangle_{\text{vertical}}} \vec{S}_i \cdot \vec{S}_j + J_1' \sum_{\langle i,j\rangle_{\text{zigzag}}} \vec{S}_i \cdot \vec{S}_j + J_2 \sum_{\langle\langle i,j\rangle\rangle} \vec{S}_i \cdot \vec{S}_j,$$

where the sums $\langle i,j\rangle$ and $\langle\langle i,j\rangle\rangle$ run over all the first- and second-neighbor bonds, respectively. The first-neighbor couplings J_1 and J_1' are for the vertical and zigzag bonds as shown in Fig. 1(a). We study most systems with $J_1' = J_1$ unless we specify otherwise. We set $J_1 = 1$ as the energy scale. By studying the spin correlations, we find a non-magnetic region sandwiched by a 120° AF phase with three sublattices for $J_2 \lesssim 0.07$ and a stripe AF phase for $J_2 \gtrsim 0.15$ as shown in Fig. 1. In this non-magnetic region, we identify two ground states with distinct properties in two sectors, indicating two competing candidates for SL phases. The spin and dimer correlations decay exponentially with small correlation lengths.

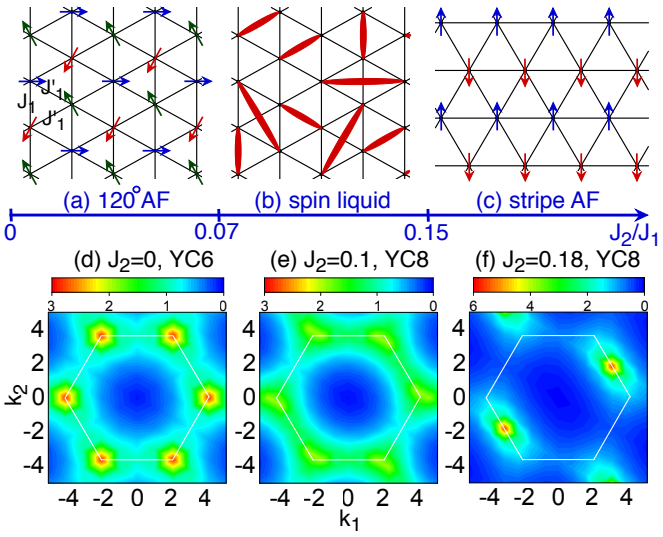

FIG. 1: (color online) Quantum phase diagram of the isotropic spin-1/2 J_1-J_2 Heisenberg model on triangular lattice ($J_1 = J_1'$). With growing J_2, the system has a 120° AF phase for $J_2 \lesssim 0.07$, a stripe AF phase for $J_2 \gtrsim 0.15$, and a SL phase in between. The schematic figures of the different phases also show the YC (a,b) and XC (c) cylinder geometries. (d)-(f) are the contour plots of spin structure factor for each phase.

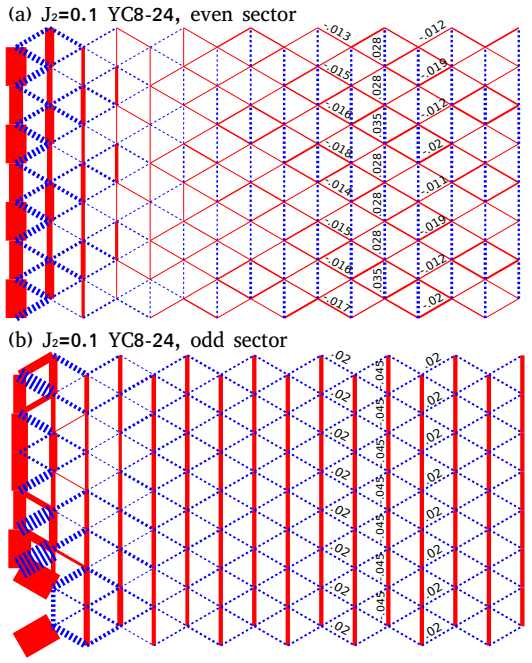

FIG. 2: (color online) The NN bond energy $\langle S_i \cdot S_j \rangle$ for $J_2 = 0.1$ on the YC8-24 cylinder in (a) the even and (b) the odd sector. The left 16 columns are shown here. The odd sector is obtained by removing one site in each boundary of cylinder. In both figures, all the bond energy have subtracted the average value -0.18. The red solid and blue dashed bonds denote the negative and positive bond energies after subtraction (with some numbers shown for clarity).

Interestingly, the chiral correlations decay exponentially fast for the ground state in the odd sector with an edge spinon, while it develops the long-range correlations in the even sector (with no spinon) for finite-size systems, consistent with the level crossing between two SLs for the systems with different boundaries. The fractionalized spinon is detected through adiabatically inserting spin flux. While the state in the odd sector agrees with a TRS preserving SL, the TRS breaking SL (e.g., chiral SL) may be a competing or nearby state in more extended parameter space. Moreover, the strong anisotropy of bond energy along different directions is observed for some finite-size systems, which may imply a nematic order for gapped Z_2 SL [70]. This possible Z_2 SL is observed to be stabilized by a small bond coupling anisotropy ($J_1' \gtrsim J_1$), which suppresses chiral order in both sectors.

We study the cylinder systems using highly accurate $SU(2)$ DMRG [71, 72] for most of calculations and $U(1)$ DMRG [71] for inserting flux [40]. Two cylinder geometries known as XC and YC are studied, which have one lattice direction parallel to the x or y axis as shown in Fig. 1. We denote them as XCL_y-L_x (YCL_y-L_x), where L_y and L_x are the number of sites along the y and x directions, respectively. We study the cylinder systems with L_y up to 10 lattice spacings by keeping up to 20000 $U(1)$-equivalent states in $SU(2)$ DMRG and 5000 states for inserting flux. The truncation errors are less than 10^{-5} in all calculations, which leads to accurate results.

Even and odd topological sectors.— Based on the resonating valence-bond picture, the ground states of SL on cylinder can be either in the even or odd sector according to the parity of the number of bonds that are cut by a vertical line along the enclosed direction. Usually, the odd sector can be obtained by removing or adding one site on each open edge of cylinder, which has been used successfully to find different sectors of the gapped SLs in kagome systems [33, 73, 74].

By doing simulations without and with removing one site at each boundary, we always find different ground states in these two sectors on YC cylinders ($L_y = 6, 8, 10$), which are shown in Fig. 2 for YC8 cylinder as an example (See Supplemental Material for YC10 cylinder) [75]. We find that the two sectors have the different bond energy distributions in the bulk of cylinder. While the vertical bonds are weaker in the even sector, they become the stronger ones in the odd sector as shown in Fig. 2. The nematic order, which is defined as the difference between the strong and weak bonds to describe the lattice rotational symmetry breaking, exhibits the distinct behaviors for the two states on our studied systems. While the nematic order grows with increased cylinder width in the odd sector, it decreases in the even sector [75].

Characteristic properties of different SL states.— Next, we further characterize the two states by studying correlation functions. In Fig. 3(a) we show the spin correlations for $J_2 = 0.1$, which decay faster with growing cylinder width in both states, indicating the vanishing spin order in both states. In Fig. 3(b), we demonstrate the dimer correlation function $D_{(ij),(kl)} = \langle (S_i \cdot S_j)(S_k \cdot S_l) \rangle - \langle S_i \cdot S_j \rangle \langle S_k \cdot S_l \rangle$, which also decay exponentially to vanish. Interestingly, the states

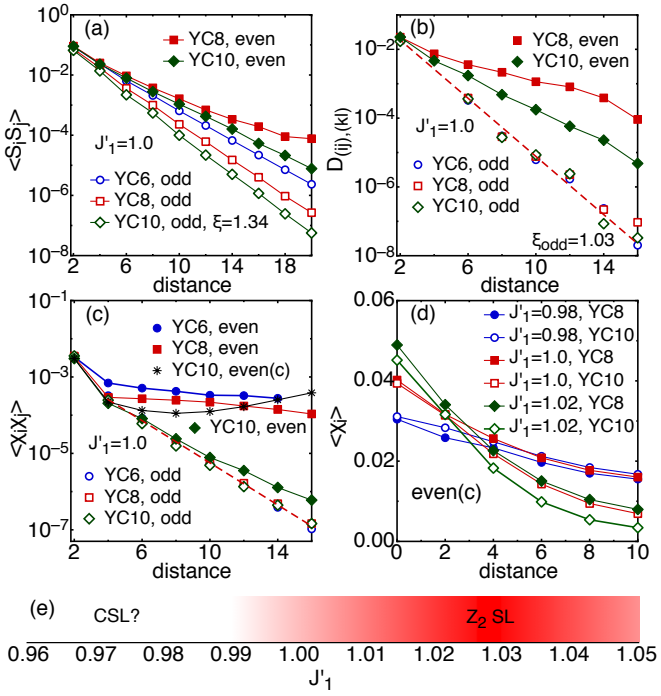

FIG. 3: (color online) (a) and (b) are the spin and dimer correlation functions on different YC cylinders for $J_2 = 0.1$. ξ denotes the corresponding correlation lengths on YC10 cylinder in the odd sector. (c) Chiral correlations for $J_2 = 0.1$ on different cylinders. All the data are obtained from real number DMRG calculations except "YC10, even(c)", which denotes the data obtained from complex wave function DMRG calculations on YC10 cylinder in the even sector. (d) Chiral order from the boundary to the bulk for the bond anisotropic system in the even sector, which are obtained from the complex DMRG. (e) Schematic phase diagram for the bond anisotropic system at $J_2 = 0.1$.

in the odd sector have very short correlation lengths almost independent of the system width. But in the even sector, the correlation lengths are longer than those in the odd sector for the smaller $L_y = 6$ and 8, which decrease with growing system width.

To study the possible TRS breaking, we calculate the scalar chiral correlation function $\langle \chi_i \chi_j \rangle$ ($\chi_i = (S_{i,1} \times S_{i,2}) \cdot S_{i,3}$). In both sectors, the chiral order has the same pattern, where the up and down triangles have the same chirality direction. As shown in Fig. 3(c), in the odd sector, the chiral correlations decay quite fast to vanish without developing long-range order. However, the chiral order and spontaneous TRS breaking are very robust for the $L_y = 6, 8$ systems in the even sector at the intermediate phase, where additional two fold ground state degeneracy is also obtained in the DMRG simulation for each system (with opposite chirality) associated with the TRS breaking. As we increase system width to $L_y = 10$, the chiral correlation becomes less robust, where different results are obtained depending on if we use complex or real initial wave function in DMRG simulation. The chiral correlation remains to be long-ranged in the complex wave function, where the TRS is spontaneously broken. However, if we use real number wave function, the DMRG will find a state with short-range chiral correlations (the real state has near identical bulk energy as the complex state but higher energy near the edge).

J_2,YCL_y	$e_{\rm even}$	$e_{\rm odd}$	Δe	$\Delta_{\rm T}$	$\Delta_{\rm S}$
0.1,YC6	-0.5155	-0.5210	0.0055	0.365	0.30
0.1,YC8	-0.5171	-0.5195	0.0024	0.335	0.26
0.1,YC10	$-0.5181(2)$	-0.5177	$-0.0004(2)$	0.30(1)	0.18
0.125,YC6	-0.5104	-0.5145	0.0041	0.389	0.33
0.125,YC8	-0.5115	-0.5133	0.0018	0.343	0.22
0.125,YC10	$-0.5119(2)$	-0.5120	0.0001(2)	0.30(1)	0.15

TABLE I: The bulk energy per site in the even ($e_{\rm even}$) and odd ($e_{\rm odd}$) sectors, the energy difference $\Delta e = e_{\rm even} - e_{\rm odd}$, the spin triplet ($\Delta_{\rm T}$) and singlet ($\Delta_{\rm S}$) gaps in the odd sector for $J_2 = 0.1$ and 0.125 on the YCL_y ($L_y = 6, 8, 10$) cylinders. We use the fully converged results for $L_y = 6$ and 8, and the extrapolated results for $L_y = 10$ as shown in Fig. 4.

To further clarify the chiral order in the system, we consider a bond anisotropy perturbation by tuning the nearest-neighbor zigzag bond strength as J_1' (see Fig. 1(a)). For $J_2 = 0.1$, we find that the SL region persists for $0.95 < J_1' < 1.05$. In the odd sector, the chiral order vanishes, and all the properties are consistent with $J_1' = 1.0$. In the even sector, the chiral order appears stronger for $0.95 < J_1' \lesssim 0.99$, where it grows a bit from YC8 to YC10 cylinder (see Fig. 3(d) for $J_1' = 0.98$). For $J_1' \gtrsim 1.0$, the chiral order decays pretty fast from the boundary to the bulk especially for the larger YC10 cylinder, which indicates a possible vanishing of the chiral order in this region in the thermodynamic limit. At $J_1' = 1.0$, the chiral correlations are strong and show long-range behavior, but the chiral order also decays with the increase of system width. Thus, the two states in both sectors may recover TRS at large system limit for $1.0 \lesssim J_1' < 1.05$, which is the most possible region for stabilizing a Z_2 SL. On the other hand, for $0.95 < J_1' \lesssim 0.99$, chiral order becomes stable in the even sector, while the fate of such a phase remains unclear depending on if the chiral order would develop in the spinon sector in the thermodynamic limit. We illustrate our finding in the phase diagram Fig. 3(e).

We calculate the bulk ground-state energy in both sectors. The energy per site for different systems are presented in Table I for $J_2 = 0.1, 0.125$. For the smaller system widths ($L_y = 6$ and 8), the odd sectors generally have the lower energy than the even sectors, which lead to a positive energy splitting $\Delta e = e_{\rm even} - e_{\rm odd}$. However, this splitting drops very fast with the increase of L_y, which is tiny for system width $L_y = 10$ (for example $\Delta e \simeq -0.0004$ for $J_2 = 0.1$, see Fig. 4) indicating the close energy for states in both sectors. We also compute the singlet Δ_s and triplet Δ_T gaps by obtaining the ground state first and then sweeping the two low-lying states simultaneously or the $S = 1$ sector in the bulk of cylinder [67]. The results are shown in Table I.

Inserting flux and the nature of different sectors.— Inserting flux is an effective way to find different sectors and to deter-

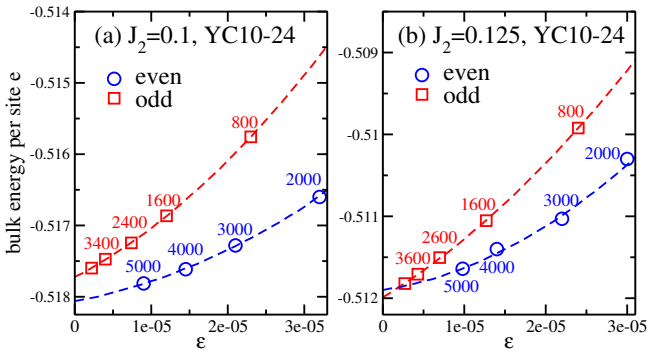

FIG. 4: (color online) Bulk energy per site e versus DMRG truncation error ε for the ground states in the even and odd sectors for (a) $J_2 = 0.1$ and (b) $J_2 = 0.125$ on the YC10-24 cylinder. The numbers denote the kept $SU(2)$ states. The energy data are fitted using the formula $e(\varepsilon) = e(0) + a\varepsilon + b\varepsilon^2$.

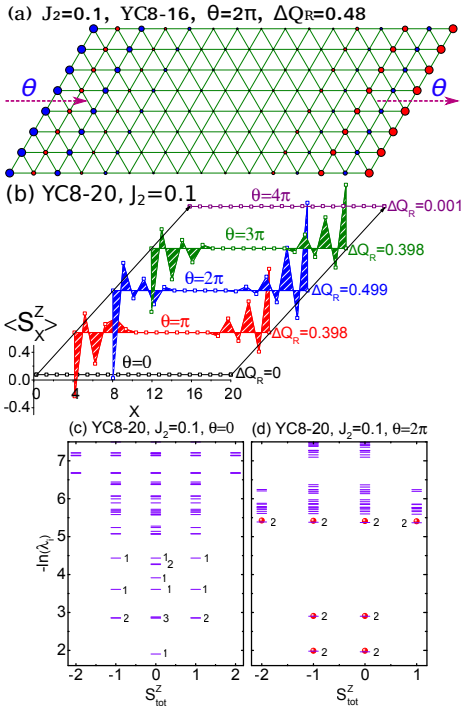

FIG. 5: (color online) (a) Real-space configuration of spin magnetization $\langle S_i^z \rangle$ after adiabatically inserting a flux $\theta = 2\pi$. The red and blue circles denote the positive and negative $\langle S_i^z \rangle$ with the area of circle proportional to the amplitude of $\langle S_i^z \rangle$. $\Delta Q_{\rm R}$ is the net spin accumulation on the right edge $\Delta Q_{\rm R} = \sum_i \langle S_i^z \rangle$, where i denotes the site on the right edge of the cylinder. (b) Real-space configuration of the accumulated spin magnetization in each column with increasing flux. Low-lying ES at the flux (c) $\theta = 0$ and (d) $\theta = 2\pi$. The numbers in ES denote the near-degenerate eigenvalues in the large weight levels. At $\theta = 2\pi$ in (d), all the eigenvalues are double degenerate as explicitly shown by the circles for the low-lying levels.

mine the basic properties of the quasi-particles in the ground states, which has been applied in DMRG to study different topological SLs [40, 73, 74]. To introduce a flux, we impose the twist boundary condition in the y direction by replacing terms $S_i^+ S_j^- + h.c. \rightarrow S_i^+ S_j^- e^{i\theta} + h.c.$ for all neighboring bonds crossing the y-boundary. We start from the even sector by adiabatically increasing θ and measuring the evolution of the spin-z local magnetization $\langle S_i^z \rangle$. With increasing θ, a net spin-z accumulates on the open edges as shown in Fig. 5(a), which indicates that the quasiparticle responding to the flux here must carry spin, such as the spinon in chiral spin liquid [40] and the fermionic spinon (spinon bonded with vison) in Z_2 SL [73, 76, 77].

With the flux $\theta = 0 \rightarrow 2\pi$, the net spin grows continuously from 0 to 0.5 on the edges as shown in Fig. 5(b). At $\theta = 2\pi$, an $S^z = \pm 1/2$ spinon develops on each boundary, and the ground state evolves to a new sector. By further increasing $\theta = 2\pi \rightarrow 4\pi$, the net spin dissipates continuously to zero, and the system evolves back to the even sector. In Figs. 5(c) and 5(d), we demonstrate the entanglement spectrum (ES) with inserting flux. At $\theta = 0$ in the even sector, the whole ES is symmetric about $S^z = 0$. At $\theta = 2\pi$, the ES evolves to be symmetric about $S^z = 1/2$, which is consistent with the observed fractionalized spin-carrying quasiparticles on boundaries. At $\theta = 4\pi$, the ES becomes the same as that at $\theta = 0$, indicating that the system evolves back to the even sector. Interestingly, each eigenvalue of the ES at $\theta = 2\pi$ is doubly degenerate. By comparing the odd sector obtained by removing sites and the sector with inserted flux $\theta = 2\pi$, we find that these two states have the same bulk energy and ES, indicating that the two sectors obtained by different methods are exactly the same. This odd sector might be consistent with the fermionic spinon sector of the Z_2 SL [76–78].

Summary and Discussions.— By means of DMRG calculations on wide cylinder systems (up to $L_y = 10$ lattice sites) of the spin-1/2 J_1-J_2 Heisenberg model on the triangular lattice, we find a SL region bordered by a 120° Néel AF phase at small $J_2 \lesssim 0.07$ and a stripe AF phase for $J_2 \gtrsim 0.15$. The spin and dimer correlations are shown to decay fast for wider systems with small correlation lengths comparable to lattice constant with large spin and singlet excitation gaps. The ES in the odd sector could be consistent with the theoretical description of the fermionic spinon in the topological theory of Z_2 SL. However, the long-range chiral correlation is observed to be strong in the even sector for a space isotropic model. By tuning the anisotropic bond coupling, we find that the possible gapped Z_2 SL is stabilized by some weak anisotropy ($J_1' \sim 1.02$). The chiral correlations are enhanced in the even sector by the opposite anisotropy ($J_1' \sim 0.98$), which may be stabilized in both sectors by TRS breaking terms and we leave this open issue for future studies.

We acknowledge the stimulating discussions with T. Senthil, X. G. Wen, Z. Y. Zhu, S. R. White, F. Wang, and Y. Qi. This research is supported by the National Science Foundation through grants PREM DMR-1205734 (W.J.H.) and DMR-1408560 (S.S.G.), and the U.S. Department of Energy, Office of Basic Energy Sciences under grant No. DE-FG02-06ER46305 (W.Z., D.N.S.).

Note added.—While completing this work, we became aware of some related papers [69, 79]. We reached the similar conclusion on gapped SL with Ref. [69].

* Electronic address: shoushu.gong@gmail.com

[1] L. Balents, Nature (London) **464**, 199 (2010), URL http://www.nature.com/nature/journal/v464/n7286/full/nature08917.html.

[2] P. W. Anderson, Mater. Res. Bull. **8**, 153 (1973), URL http://www.sciencedirect.com/science/article/pii/0025540873901670.

[3] P. A. Lee, N. Nagaosa, and X.-G. Wen, Rev. Mod. Phys. **78**, 17 (2006), URL http://link.aps.org/doi/10.1103/RevModPhys.78.17.

[4] X. G. Wen, Phys. Rev. B **40**, 7387 (1989), URL http://link.aps.org/doi/10.1103/PhysRevB.40.7387.

[5] X. G. Wen and Q. Niu, Phys. Rev. B **41**, 9377 (1990), URL http://link.aps.org/doi/10.1103/PhysRevB.41.9377.

[6] X.-G. Wen, International Journal of Modern Physics B **4**, 239 (1990), URL http://www.worldscientific.com/doi/abs/10.1142/S0217979290000139.

[7] X. G. Wen, Phys. Rev. B **44**, 2664 (1991), URL http://link.aps.org/doi/10.1103/PhysRevB.44.2664.

[8] T. Senthil and M. P. A. Fisher, Phys. Rev. B **62**, 7850 (2000), URL http://link.aps.org/doi/10.1103/PhysRevB.62.7850.

[9] T. Senthil and M. P. A. Fisher, Phys. Rev. Lett. **86**, 292 (2001), URL http://link.aps.org/doi/10.1103/PhysRevLett.86.292.

[10] D. S. Rokhsar and S. A. Kivelson, Phys. Rev. Lett. **61**, 2376 (1988), URL http://link.aps.org/doi/10.1103/PhysRevLett.61.2376.

[11] N. Read and S. Sachdev, Phys. Rev. Lett. **66**, 1773 (1991), URL http://link.aps.org/doi/10.1103/PhysRevLett.66.1773.

[12] R. Moessner and S. L. Sondhi, Phys. Rev. Lett. **86**, 1881 (2001), URL http://link.aps.org/doi/10.1103/PhysRevLett.86.1881.

[13] L. Balents, M. P. A. Fisher, and S. M. Girvin, Phys. Rev. B **65**, 224412 (2002), URL http://link.aps.org/doi/10.1103/PhysRevB.65.224412.

[14] T. Senthil and O. Motrunich, Phys. Rev. B **66**, 205104 (2002), URL http://link.aps.org/doi/10.1103/PhysRevB.66.205104.

[15] O. I. Motrunich and T. Senthil, Phys. Rev. Lett. **89**, 277004 (2002), URL http://link.aps.org/doi/10.1103/PhysRevLett.89.277004.

[16] D. N. Sheng and L. Balents, Phys. Rev. Lett. **94**, 146805 (2005), URL http://link.aps.org/doi/10.1103/PhysRevLett.94.146805.

[17] A. Kitaev, Annals of Physics **321**, 2 (2006), URL http://www.sciencedirect.com/science/article/pii/S0003491605002381.

[18] H. Yao and S. A. Kivelson, Phys. Rev. Lett. **99**, 247203 (2007), URL http://link.aps.org/doi/10.1103/PhysRevLett.99.247203.

[19] D. F. Schroeter, E. Kapit, R. Thomale, and M. Greiter, Phys. Rev. Lett. **99**, 097202 (2007), URL http://link.aps.org/doi/10.1103/PhysRevLett.99.097202.

[20] S. V. Isakov, M. B. Hastings, and R. G. Melko, Nature Physics **7**, 772 (2011), 1102.1721, URL http://www.nature.com/nphys/journal/v7/n10/abs/nphys2036.html.

[21] P. Mendels, F. Bert, M. A. de Vries, A. Olariu, A. Harrison, F. Duc, J. C. Trombe, J. S. Lord, A. Amato, and C. Baines, Phys. Rev. Lett. **98**, 077204 (2007), URL http://link.aps.org/doi/10.1103/PhysRevLett.98.077204.

[22] J. S. Helton, K. Matan, M. P. Shores, E. A. Nytko, B. M. Bartlett, Y. Yoshida, Y. Takano, A. Suslov, Y. Qiu, J.-H. Chung, et al., Phys. Rev. Lett. **98**, 107204 (2007), URL http://link.aps.org/doi/10.1103/PhysRevLett.98.107204.

[23] M. A. de Vries, J. R. Stewart, P. P. Deen, J. O. Piatek, G. J. Nilsen, H. M. Rønnow, and A. Harrison, Phys. Rev. Lett. **103**, 237201 (2009), URL http://link.aps.org/doi/10.1103/PhysRevLett.103.237201.

[24] B. Fåk, E. Kermarrec, L. Messio, B. Bernu, C. Lhuillier, F. Bert, P. Mendels, B. Koteswararao, F. Bouquet, J. Ollivier, et al., Phys. Rev. Lett. **109**, 037208 (2012), URL http://link.aps.org/doi/10.1103/PhysRevLett.109.037208.

[25] T.-H. Han, J. S. Helton, S. Chu, D. G. Nocera, J. A. Rodriguez-Rivera, C. Broholm, and Y. S. Lee, Nature (London) **492**, 406 (2012), URL http://www.nature.com/nature/journal/v492/n7429/full/nature11659.html.

[26] Y. Shimizu, K. Miyagawa, K. Kanoda, M. Maesato, and G. Saito, Phys. Rev. Lett. **91**, 107001 (2003), URL http://link.aps.org/doi/10.1103/PhysRevLett.91.107001.

[27] Y. Kurosaki, Y. Shimizu, K. Miyagawa, K. Kanoda, and G. Saito, Phys. Rev. Lett. **95**, 177001 (2005), URL http://link.aps.org/doi/10.1103/PhysRevLett.95.177001.

[28] S. Yamashita, Y. Nakazawa, M. Oguni, Y. Oshima, H. Nojiri, Y. Shimizu, K. Miyagawa, and K. Kanoda, Nature Physics **4**, 459 (2008), URL http://www.nature.com/nphys/journal/v4/n6/abs/nphys942.html.

[29] M. Yamashita, N. Nakata, Y. Kasahara, T. Sasaki, N. Yoneyama, N. Kobayashi, S. Fujimoto, T. Shibauchi, and Y. Matsuda, Nature Physics **5**, 44 (2009), URL http://www.nature.com/nphys/journal/v5/n1/full/nphys1134.html.

[30] T. Itou, A. Oyamada, S. Maegawa, M. Tamura, and R. Kato, Phys. Rev. B **77**, 104413 (2008), URL http://link.aps.org/doi/10.1103/PhysRevB.77.104413.

[31] M. Yamashita, N. Nakata, Y. Senshu, M. Nagata, H. M. Yamamoto, R. Kato, T. Shibauchi, and Y. Matsuda, Science **328**, 1246 (2010), URL http://www.sciencemag.org/content/328/5983/1246.full.

[32] H. C. Jiang, Z. Y. Weng, and D. N. Sheng, Phys. Rev. Lett. **101**, 117203 (2008), URL http://link.aps.org/doi/10.1103/PhysRevLett.101.117203.

[33] S. Yan, D. A. Huse, and S. R. White, Science **332**, 1173 (2011), URL http://www.sciencemag.org/content/332/6034/1173.full.

[34] S. Depenbrock, I. P. McCulloch, and U. Schollwöck, Phys. Rev. Lett. **109**, 067201 (2012), URL http://link.aps.org/doi/10.1103/PhysRevLett.109.067201.

[35] H.-C. Jiang, Z. Wang, and L. Balents, Nature Physics **8**, 902 (2012), URL http://www.nature.com/nphys/journal/v8/n12/full/nphys2465.html.

[36] Y. Ran, M. Hermele, P. A. Lee, and X.-G. Wen, Phys. Rev. Lett.

98, 117205 (2007), URL http://link.aps.org/doi/10.1103/PhysRevLett.98.117205.

[37] Y. Iqbal, F. Becca, S. Sorella, and D. Poilblanc, Phys. Rev. B **87**, 060405 (2013), URL http://link.aps.org/doi/10.1103/PhysRevB.87.060405.

[38] Y. Iqbal, D. Poilblanc, and F. Becca, Phys. Rev. B **89**, 020407 (2014), URL http://link.aps.org/doi/10.1103/PhysRevB.89.020407.

[39] L. Messio, B. Bernu, and C. Lhuillier, Phys. Rev. Lett. **108**, 207204 (2012), URL http://link.aps.org/doi/10.1103/PhysRevLett.108.207204.

[40] S.-S. Gong, W. Zhu, and D. Sheng, Scientific reports **4**, 6317 (2014), URL http://www.nature.com/srep/2014/140910/srep06317/full/srep06317.html.

[41] Y.-C. He, D. N. Sheng, and Y. Chen, Phys. Rev. Lett. **112**, 137202 (2014), URL http://link.aps.org/doi/10.1103/PhysRevLett.112.137202.

[42] B. Bauer, L. Cincio, B. P. Keller, M. Dolfi, G. Vidal, S. Trebst, and A. W. W. Ludwig, Nature Communications **5**, 5137 (2014), URL http://www.nature.com/ncomms/2014/141010/ncomms6137/abs/ncomms6137.html.

[43] V. Kalmeyer and R. B. Laughlin, Phys. Rev. Lett. **59**, 2095 (1987), URL http://link.aps.org/doi/10.1103/PhysRevLett.59.2095.

[44] X. G. Wen, F. Wilczek, and A. Zee, Phys. Rev. B **39**, 11413 (1989), URL http://link.aps.org/doi/10.1103/PhysRevB.39.11413.

[45] R. Ganesh, J. van den Brink, and S. Nishimoto, Phys. Rev. Lett. **110**, 127203 (2013), URL http://link.aps.org/doi/10.1103/PhysRevLett.110.127203.

[46] Z. Zhu, D. A. Huse, and S. R. White, Phys. Rev. Lett. **110**, 127205 (2013), URL http://link.aps.org/doi/10.1103/PhysRevLett.110.127205.

[47] S.-S. Gong, D. N. Sheng, O. I. Motrunich, and M. P. A. Fisher, Phys. Rev. B **88**, 165138 (2013), URL http://link.aps.org/doi/10.1103/PhysRevB.88.165138.

[48] S.-S. Gong, W. Zhu, D. N. Sheng, O. I. Motrunich, and M. P. A. Fisher, Phys. Rev. Lett. **113**, 027201 (2014), URL http://link.aps.org/doi/10.1103/PhysRevLett.113.027201.

[49] S. Sachdev, Phys. Rev. B **45**, 12377 (1992), URL http://link.aps.org/doi/10.1103/PhysRevB.45.12377.

[50] B. Bernu, C. Lhuillier, and L. Pierre, Phys. Rev. Lett. **69**, 2590 (1992), URL http://link.aps.org/doi/10.1103/PhysRevLett.69.2590.

[51] L. Capriotti, A. E. Trumper, and S. Sorella, Phys. Rev. Lett. **82**, 3899 (1999), URL http://link.aps.org/doi/10.1103/PhysRevLett.82.3899.

[52] W. Zheng, J. O. Fjærestad, R. R. P. Singh, R. H. McKenzie, and R. Coldea, Phys. Rev. B **74**, 224420 (2006), URL http://link.aps.org/doi/10.1103/PhysRevB.74.224420.

[53] S. R. White and A. L. Chernyshev, Phys. Rev. Lett. **99**, 127004 (2007), URL http://link.aps.org/doi/10.1103/PhysRevLett.99.127004.

[54] O. I. Motrunich, Phys. Rev. B **72**, 045105 (2005), URL http://link.aps.org/doi/10.1103/PhysRevB.72.045105.

[55] D. N. Sheng, O. I. Motrunich, and M. P. A. Fisher, Phys. Rev. B **79**, 205112 (2009), URL http://link.aps.org/doi/10.1103/PhysRevB.79.205112.

[56] M. S. Block, R. V. Mishmash, R. K. Kaul, D. N. Sheng, O. I. Motrunich, and M. P. A. Fisher, Phys. Rev. Lett. **106**, 046402 (2011), URL http://link.aps.org/doi/10.1103/PhysRevLett.106.046402.

[57] G. Misguich, C. Lhuillier, B. Bernu, and C. Waldtmann, Phys. Rev. B **60**, 1064 (1999), URL http://link.aps.org/doi/10.1103/PhysRevB.60.1064.

[58] T. Jolicoeur, E. Dagotto, E. Gagliano, and S. Bacci, Phys. Rev. B **42**, 4800 (1990), URL http://link.aps.org/doi/10.1103/PhysRevB.42.4800.

[59] A. V. Chubukov and T. Jolicoeur, Phys. Rev. B **46**, 11137 (1992), URL http://link.aps.org/doi/10.1103/PhysRevB.46.11137.

[60] L. O. Manuel and H. A. Ceccatto, Phys. Rev. B **60**, 9489 (1999), URL http://link.aps.org/doi/10.1103/PhysRevB.60.9489.

[61] R. V. Mishmash, J. R. Garrison, S. Bieri, and C. Xu, Phys. Rev. Lett. **111**, 157203 (2013), URL http://link.aps.org/doi/10.1103/PhysRevLett.111.157203.

[62] R. Kaneko, S. Morita, and M. Imada, Journal of the Physical Society of Japan **83** (2014), URL http://journals.jps.jp/doi/abs/10.7566/JPSJ.83.093707.

[63] P. H. Y. Li, R. F. Bishop, and C. E. Campbell, Phys. Rev. B **91**, 014426 (2015), URL http://link.aps.org/doi/10.1103/PhysRevB.91.014426.

[64] S. Yunoki and S. Sorella, Phys. Rev. B **74**, 014408 (2006), URL http://link.aps.org/doi/10.1103/PhysRevB.74.014408.

[65] M. Q. Weng, D. N. Sheng, Z. Y. Weng, and R. J. Bursill, Phys. Rev. B **74**, 012407 (2006), URL http://link.aps.org/doi/10.1103/PhysRevB.74.012407.

[66] O. A. Starykh, H. Katsura, and L. Balents, Phys. Rev. B **82**, 014421 (2010), URL http://link.aps.org/doi/10.1103/PhysRevB.82.014421.

[67] A. Weichselbaum and S. R. White, Phys. Rev. B **84**, 245130 (2011), URL http://link.aps.org/doi/10.1103/PhysRevB.84.245130.

[68] K. Li, S.-L. Yu, and J.-X. Li, ArXiv e-prints (2014), 1409.7820, URL http://arxiv.org/abs/1409.7820.

[69] Z. Zhu and S. R. White, Phys. Rev. B **92**, 041105 (2015), URL http://link.aps.org/doi/10.1103/PhysRevB.92.041105.

[70] K. Slagle and C. Xu, Phys. Rev. B **89**, 104418 (2014), URL http://link.aps.org/doi/10.1103/PhysRevB.89.104418.

[71] S. R. White, Phys. Rev. Lett. **69**, 2863 (1992), URL http://link.aps.org/doi/10.1103/PhysRevLett.69.2863.

[72] I. McCulloch and M. Gulácsi, Europhysics Letters **57**, 852 (2002), URL http://iopscience.iop.org/0295-5075/57/6/852.

[73] Y.-C. He, D. N. Sheng, and Y. Chen, Phys. Rev. B **89**, 075110 (2014), URL http://link.aps.org/doi/10.1103/PhysRevB.89.075110.

[74] W. Zhu, S. Gong, and D. Sheng, Journal of Statistical Mechanics: Theory and Experiment **2014**, P08012 (2014), URL http://iopscience.iop.org/1742-5468/2014/8/P08012.

[75] See Supplemental Material for more details.

[76] Y. Qi and L. Fu, Phys. Rev. B **91**, 100401 (2015), URL http://link.aps.org/doi/10.1103/PhysRevB.91.100401.

[77] M. Zaletel, Y.-M. Lu, and A. Vishwanath, ArXiv e-prints (2015), 1501.01395, URL http://arxiv.org/abs/1501.01395.

[78] M. P. Zaletel and A. Vishwanath, Phys. Rev. Lett. **114**, 077201

(2015), URL http://link.aps.org/doi/10.1103/PhysRevLett.114.077201.

[79] S. N. Saadatmand, B. J. Powell, and I. P. McCulloch, Phys. Rev. B **91**, 245119 (2015), URL http://link.aps.org/doi/10.1103/PhysRevB.91.245119.

Supplemental Material: Competing Spin Liquid States in the Spin-$1/2$ Heisenberg Model On Triangular Lattice

I. Correlation functions

First of all, we demonstrate the spin and dimer correlation functions for different J_2 on YC8-24 cylinder as shown in Fig. 6. In this figure, the correlation functions for $J_2 = 0.1$ and 0.125 are shown in the odd sector. In Fig. 6(a), the spin correlations $|\langle S_i \cdot S_j \rangle|$ decay slowly as a function of distance for $J_2 = 0$, 0.05, and 0.18, indicating the long-range magnetic order; instead for $J_2 = 0.1$ and 0.125, it decays exponentially to vanish, which is consistent with the absent magnetic order.

In order to investigate the possible valence-bond solid order, we study the dimer-dimer correlation function on cylinder systems, which is defined as

$$D_{(ij),(kl)} = \langle B_{ij} B_{kl} \rangle - \langle B_{ij} \rangle \langle B_{kl} \rangle, \quad (1)$$

where (i, j) and (k, l) represent the nearest-neighbor (NN) bonds, and $B_{ij} = S_i \cdot S_j$. In Fig. 7 we show the dimer correlations for $J_2 = 0.1$ on YC8-24 cylinder in both the even and odd sectors. The dimer correlation in the odd sector decays faster than that in the even sector, which is shown in Fig. 3(b) of the main text. In Fig. 6(b), we show the dimer correlations for different J_2, which all decay fast to vanish with an exponential manner.

To detect the possible time-reversal symmetry (TRS) breaking, we measure the chiral-chiral correlation functions for the four kinds of triangles Δ_1, Δ_2, Δ_3, and Δ_4 as shown in Fig. 8(a) in both the even and odd sectors. The chiral-chiral correlation function is defined as

$$\langle \chi_i \chi_j \rangle = \langle [S_{i,1} \cdot (S_{i,2} \times S_{i,3})][S_{j,1} \cdot (S_{j,2} \times S_{j,3})] \rangle, \quad (2)$$

where $\chi_i = S_{i,1} \cdot (S_{i,2} \times S_{i,3})$ is the scalar chiral order parameter of triangle Δ_i. As an example, we show the chiral correlations for $J_2 = 0.1$ on the YC8-24 cylinder in Fig. 8. In the odd sector, all the chiral correlations decay quite fast to vanish (see Fig. 8(c)), which is also observed on YC6 and YC10 cylinders and indicates no TRS breaking. However, in the even sector as shown in Fig. 8(b), the chiral correlations for the triangles Δ_1, Δ_2 and Δ_3 exhibit the long-range chiral order, while those for Δ_4 decay fast. Using the complex number DMRG, we can measure the chiral orders $\langle \chi_i \rangle$ for all the triangles directly. In the odd sector, the chiral orders for all the triangles are vanished. In the even sector, we find that the chiral orders for Δ_1, Δ_2 and Δ_3 are finite, and $\langle \chi_i \rangle$ for Δ_4 is much smaller (for $J_2 = 0.1$ on YC10 cylinder, it is about 10^{-4}). In Fig. 8(d) we show the chiral correlations of Δ_1 by keeping different $SU(2)$ DMRG states for $J_2 = 0.1$, $J_1' = 1.0$ and 0.98 on YC10 cylinder in the even sector. By increasing the kept $SU(2)$ DMRG states from 2000 to 4000, the chiral correlations change slightly, indicating the near convergence of the chiral correlations with increasing states. The non-zero chiral orders indicate the TRS breaking in the even sector.

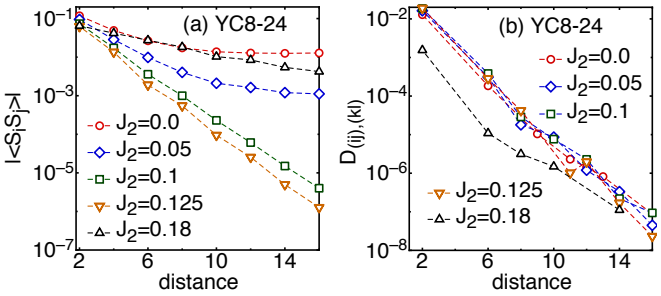

FIG. 6: (color online) (a) and (b) are the spin and dimer correlation functions for various J_2 couplings on the YC8-24 cylinder. In the spin liquid phase region, both correlation functions decay exponentially to vanish.

II. Bond energy distributions in different sectors

In Fig. 2 of the main text, we have shown the different NN bond energy distributions of the ground states in different sectors on YC8 cylinder. Here, we demonstrate the bond energy

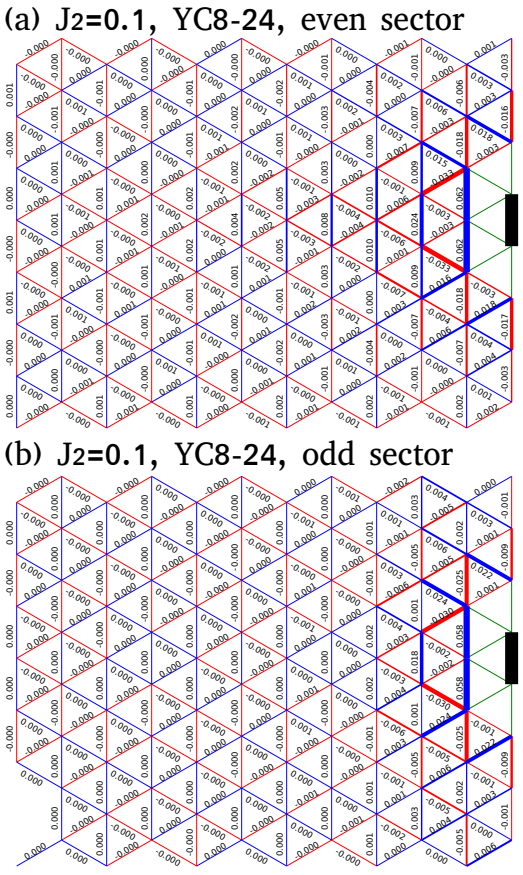

FIG. 7: (color online) The dimer-dimer correlation function for $J_2 = 0.1$ on YC8-24 cylinder in (a) the even sector and (b) the odd sector. The black bond in the middle is the reference bond. The blue and red bonds denote the positive and negative dimer correlations, respectively.

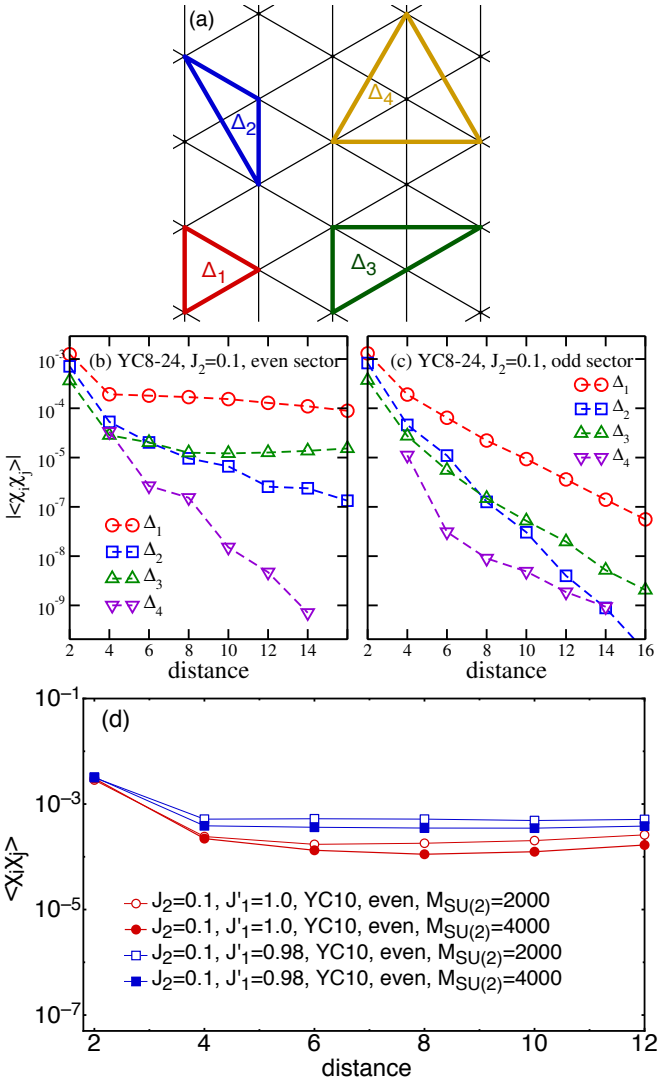

FIG. 8: (color online) (a) The four three-spin triangles which are used to calculate the chira-chiral correlation functions in (b) and (c). (b) and (c) are the chiral-chiral correlation functions versus triangle distance for $J_2 = 0.1$ on YC8-24 cylinder in the even and odd sectors. These chiral correlations are obtained from the real number DMRG. (d) is the chiral-chiral correlation functions of the triangles Δ_1 at $J_2 = 0.1$ with anisotropic bond coupling $J'_1 = 1.0$ and 0.98 in the even sector on YC10-20 cylinder with different kept $SU(2)$ DMRG states.

distributions for $J_2 = 0.1$ on YC10 cylinder in both sectors, and compare the results in the even sector obtained from the real and complex number states. As the even sector is harder to converge in DMRG calculations, we first show the bond energy distributions by keeping different states in the even sector. As shown in Fig. 9, by keeping 1000 $SU(2)$ states, both the real and complex states exhibit some sort of string pattern. In particular, the real state shown in Fig. 9(a) has much stronger fluctuations. With increasing the kept states to 2000, the fluctuations become weaker. By comparing the ground-state energy of the real and complex states by keeping the same optimal states such as $M_{SU(2)} = 2000, 3000$, we find that the two states have the near identical bulk energy, but the real state has the higher total energy as there are much stronger bond energy fluctuations on the edge. This indicates that the real wave function is less converged near the boundary.

In Fig. 10, we show the bond energy distributions obtained by keeping the most states for both the even and odd sectors, where the fluctuations are much smaller compared with the data in Fig. 9. The real and complex states in the even sector have the same pattern of the bond energy distribution in the bulk, which has the weaker vertical bonds. In contrast, the vertical bonds become the stronger bonds in the odd sector. This difference between the two sectors is consistent with our observations for YC8 cylinder, which are shown in Fig. 2 of the main text.

III. Nematic order

In Fig. 10, we notice that the NN bond energy distributions have the lattice anisotropy with different bond energy along different lattice directions. In particular, the bond energy in the odd sector seems to have a strong anisotropy as shown in Fig. 2(b) of the main text and Fig. 10(c) in Supplemental Material. The strong lattice anisotropy may indicate a lattice rotational symmetry breaking. To investigate such a possibility, we study the anisotropy on different cylinder systems. For convenience, we define the nematic order parameter (NOP) as the difference of the bond energy of the vertical bond and the others (NOP = $\text{Bond}_{\text{zigzag}}$ - $\text{Bond}_{\text{vertical}}$). In Fig. 11, we present the NOP for $J_2 = 0.1$ and 0.125 on different cylinders in two sectors, together with the results by tuning the anisotropic bond coupling J'_1. In the odd sector, the NOP increases continuously with growing system width for $L_y = 6, 8, 10$ on YC cylinder for different J'_1. On the XC8 cylinder, the systems also have strong anisotropy. These results may suggest a finite NOP in thermodynamic limit. However, in the even sector the behaviors of the NOP appear distinct for different J'_1. For $J'_1 = 1.0$ and 1.02, the negative NOP on $L_y = 6, 8, 10$ indicates the weaker vertical bonds. However, for $J'_1 = 0.98$, the vertical bonds become the stronger bonds, and the NOP decreases continuously with growing system width for $L_y = 6, 8, 10$.

IV. Entanglement Entropy

We have calculated the entanglement entropy (EE) on the $L_y = 6$, 8, 10, and 12 YC cylinders at $J_2 = 0.1$. In Figs. 12(a)∼(d), we show the entropy for $L_y = 8$, 10, and 12 cylinders by keeping different $SU(2)$ DMRG states $M_{SU(2)}$. As shown in Fig. 12(a)∼(c), by using the less accurate data with the big truncation error, the linear extrapolated EE on YC8 cylinder and in the odd sector on YC10 cylinder is far from the converged results. However, with the increasing kept

states, the truncation error decreases, and the more accurate EE is obtained. These three figures suggest that it is hard to obtain the converged EE for the wider systems. In the even sector on YC10 cylinder and odd sector on YC12 cylinder (Fig. 12(d)), we have kept up to 4000 $SU(2)$ states, however, most data have the truncation error larger than 2×10^{-5}, which indicates that they are far from convergency. By using these data, we only can obtain the lower bound of the EE with a linear fitting, and due to the big truncation error, it is hard to get the reliable topological entanglement entropy on large cylinders. Based on the entropy data for $L_y = 8$ and 10 in the odd sector with the smaller error bar, we get the topological entanglement entropy close to $\ln 2$ from a reasonable fitting as shown in Fig. 12(e), which is consistent with the gapped Z_2 spin liquid.

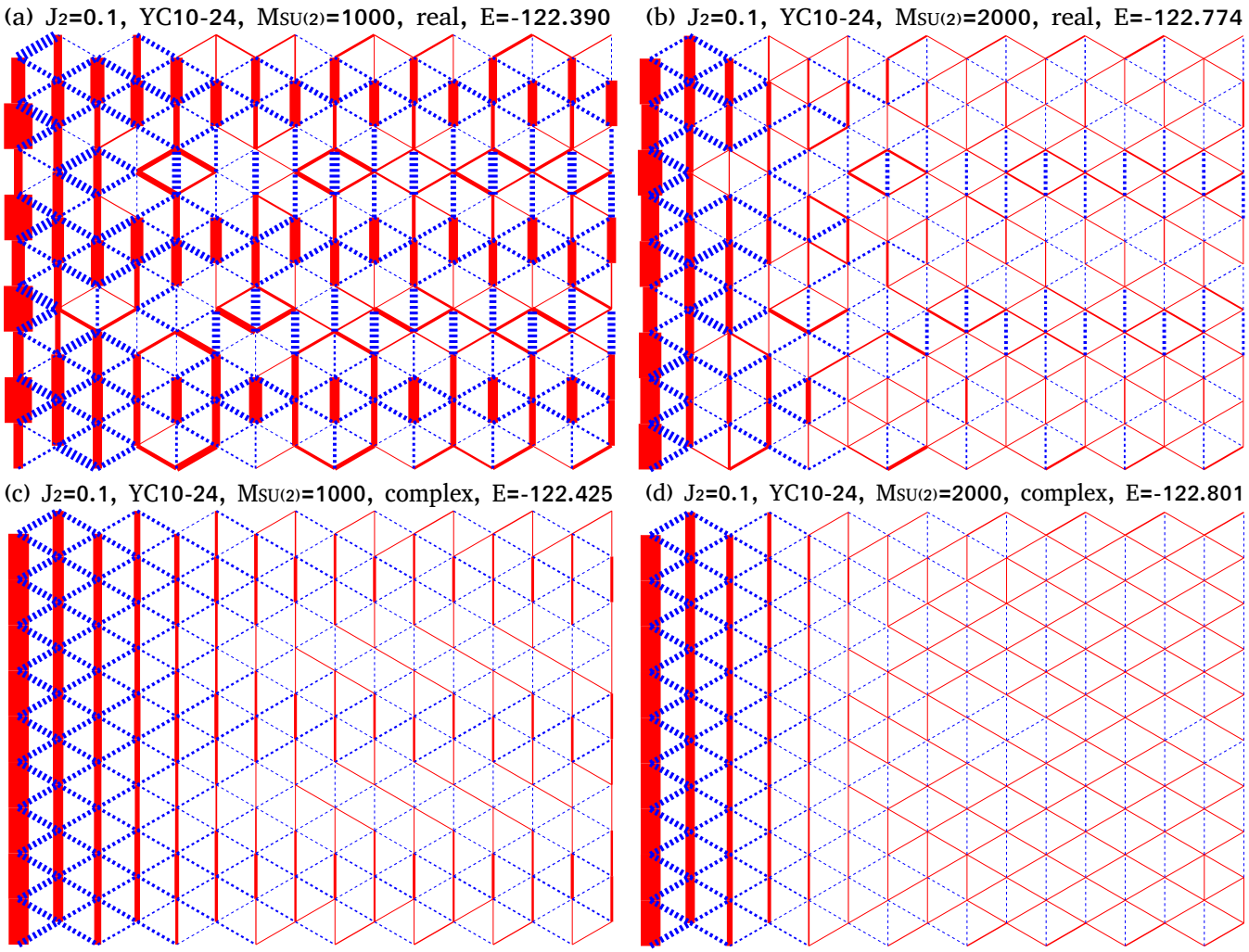

FIG. 9: (color online) The NN bond textures for the even sector of $J_2 = 0.1$ on the YC10-24 cylinder are calculated by using real [(a) and (b)] and complex [(c) and (d)] number DMRG. Different $SU(2)$ states are kept: $M_{SU(2)} = 1000$ in (a) and (c); $M_{SU(2)} = 2000$ in (b) and (d). The left 16 columns are shown here. In all figures, all the bond energy have subtracted a value -0.18. The red solid and blue dashed bonds denote the negative and positive bond textures, respectively. E is the total energy for each state.

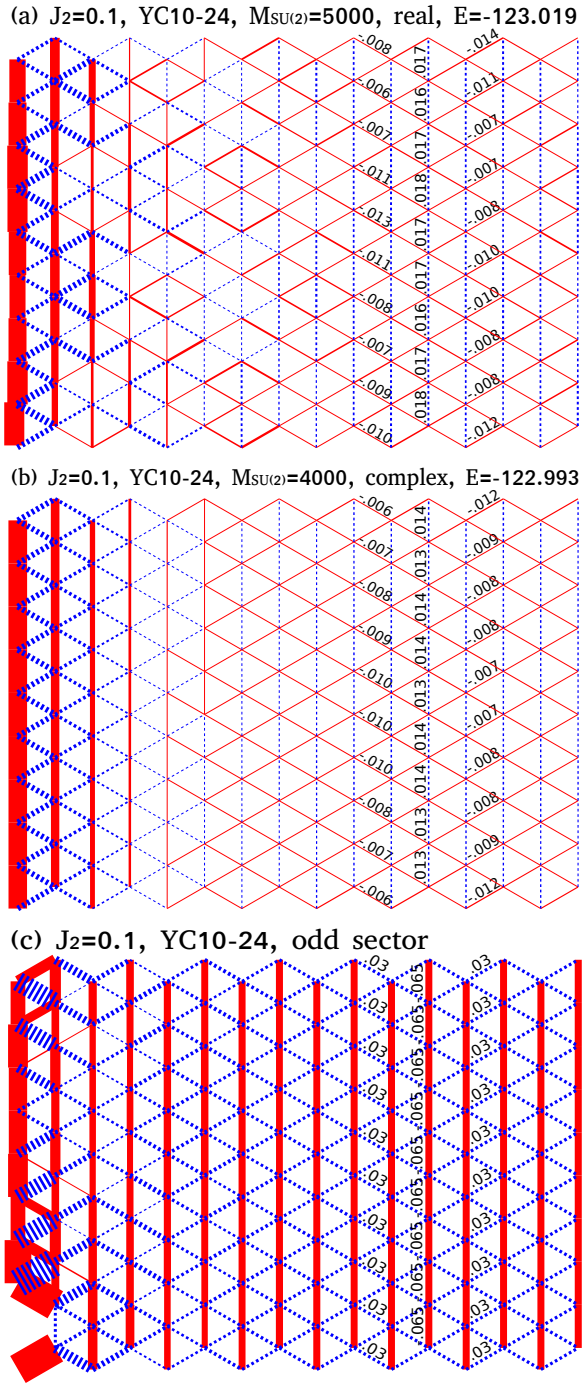

FIG. 10: (color online) The NN bond textures for $J_2 = 0.1$ on YC10 cylinders. The left 16 columns are shown here. (a) is the even sector obtained from real number DMRG by keeping 5000 $SU(2)$ states. (b) is the even sector obtained from complex number DMRG by keeping 3000 $SU(2)$ states. (c) is the odd sector obtained by removing one site in each boundary. In all figures, all the bond energy have subtracted a value -0.18. The numbers are the bond texture values. The red solid and blue dashed bonds denote the negative and positive bond textures, respectively. E is the total energy. For the system (a) by keeping 4000 $SU(2)$ states, the total energy $E = -122.978$, which is still higher than the energy of the complex state in (b).

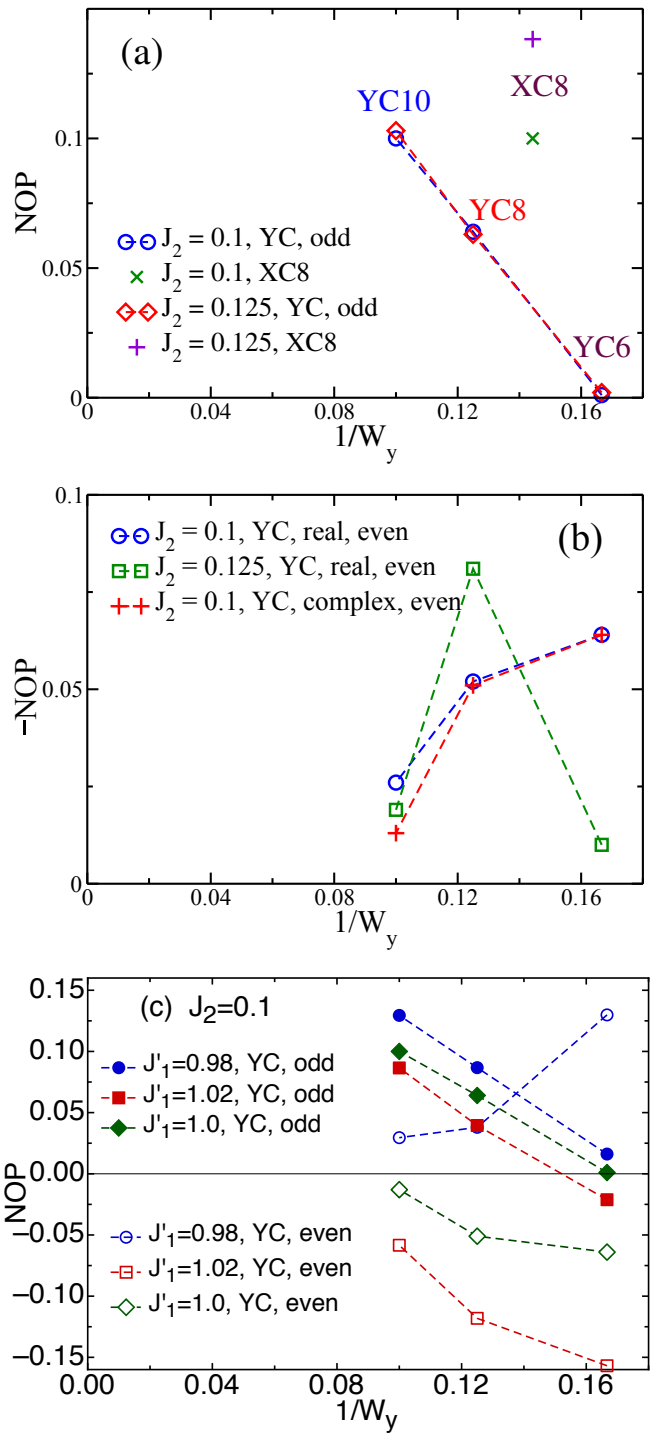

FIG. 11: (color online) Cylinder width dependence of the nematic order parameter (NOP) for $J_2 = 0.1$ and 0.125 in (a) the odd sector and (b) the even sector. In the odd sector (a), the NOP increases with growing system width. In the even sector (b), we show the NOP obtained from both real and complex number DMRG calculations, which are consistent on YC6 and YC8 cylinders. On YC10 cylinder, the complex states have the better convergence and thus exhibit the smaller fluctuations. (c) is the NOP in the even and odd sectors at $J_2 = 0.1$ with tuning the bond anisotropy J_1'.

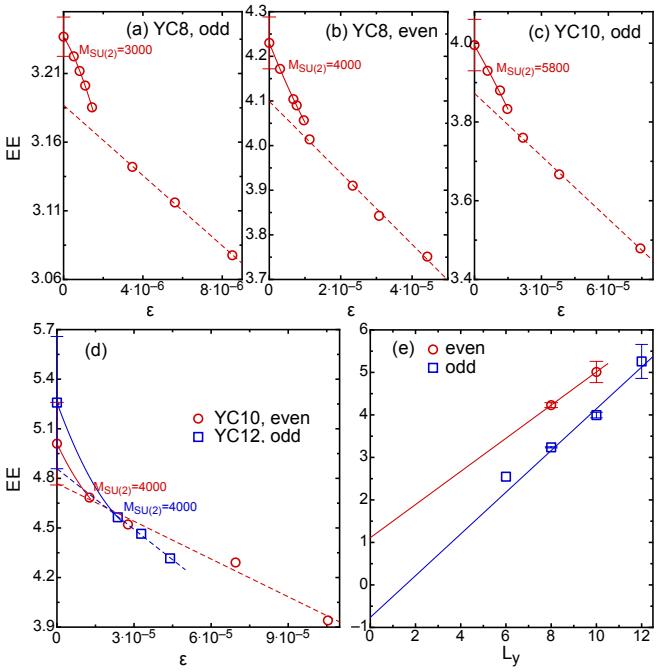

FIG. 12: (color online) (a)∼(d) The entanglement entropy as a function of the DMRG truncation error ε at $J_2 = 0.1$ on YC8, YC10, and YC12 cylinders in the even and odd sectors. The largest kept $SU(2)$ DMRG states $M_{SU(2)}$ are shown. In (a)∼(c), we show the convergency of the EE by increasing the kept states. By doing the linear fitting with the less accurate data (red dashed lines), the extrapolated entropy is far from convergence. With more accurate data, we do the quadratic fitting (red solid lines), and the error bar is the difference between the extrapolated EE and the last raw data. In (d) we show the EE in the even sector on YC10 cylinder and odd sector on YC12 cylinder. Even with 4000 SU(2) DMRG states, most of these data have the truncation error larger than 2×10^{-5}, which indicates that they are far from convergency. Based on the experience of (a)∼(c), we do the linear fitting (dashed lines) to obtain the lower bound for the EE, and also make a quadratic extrapolation (solid lines) with the guessed big error bar for these two points. (e) The width dependence of the entanglement entropy in the even and odd sectors at $J_2 = 0.1$.